INORGANIC CHEMISTRY FRONTIERS

RESEARCH ARTICLE

View Article Online
View Journal | View Issue

Cite this: *Inorg. Chem. Front.*, 2023, **10**, 4496

Modulating optical performance by phase transition in a nonlinear optical material β-$Li_2RbBi(PO_4)_2$†

Lei Wu,[a] Ruixin Zhang,[b] Qun Jing,*[b] Hongyu Huang,[a] Xianmeng He,[a] Zhongchang Wang *[c] and Zhaohui Chen *[a]

Received 4th May 2023,
Accepted 18th June 2023

DOI: 10.1039/d3qi00828b

rsc.li/frontiers-inorganic

As nonlinear optical (NLO) materials, phosphates often suffer from weak second harmonic generation (SHG) response and low birefringence. Here, we report the successful synthesis of a new UV NLO orthophosphate, β-$Li_2RbBi(PO_4)_2$, by the high temperature solution method, and demonstrate that it crystallizes in a polar space group of $P2_1$ and is composed of 1D $^1[Bi_4(PO_4)_8]_\infty$ infinite chains that are constructed from $^1[Bi_2O_{11}]_\infty$ chains and $[PO_4]$ clusters. The optical functional motifs $^1[Bi_4(PO_4)_8]_\infty$ are arranged in a parallel mode, which greatly improves the polarizability of the phosphate. As a result, β-$Li_2RbBi(PO_4)_2$ presents the largest SHG response, 5.2 × KH_2PO_4 (KDP), at 1064 nm incident radiation among all the Bi-based phosphates. Furthermore, first-principles calculations reveal that the synergistic effect of P–O and Bi–O groups contributes significantly to the optical properties of the title compound.

Introduction

Nonlinear optical (NLO) materials, which are capable of producing coherent light, can extend the application bands of laser to ultraviolet (UV) and deep-UV by frequency conversion technology. This is of particular importance in high-tech fields, such as all-solid-state semiconductor manufacturing, photolithography, laser system, attosecond pulse generation, and ultra-high resolution photoemission spectroscopy.[1–5] Over the past decades, great efforts have been devoted to exploring UV/deep-UV NLO materials with excellent performance.[6–10]

Currently, potential NLO materials are mostly limited to π-conjugated systems, especially for borates, carbonates, and nitrates. Consequently, a number of second harmonic generation (SHG) materials were discovered.[11–16] However, taking into account large SHG, short cutoff edge, and appropriate birefringence is always the persistent core target.[17,18] In order to meet the above conditions, introducing strong electronegativity primitives, such as fluorine, might optimize the optical properties and provide an effective strategy for designing excellent NLO materials. As a result, many prominent UV/deep-UV NLO crystals have been reported, including AB_4O_6F (A = K, Rb, Cs, and NH_4),[19–21] $MB_5O_7F_3$ (M = Sr, Mg),[22,23] $ABCO_3F$ (A = K, Rb, Cs; B = Ca, Sr, Mg),[24,25] *etc*. Non-π-conjugated systems, such as phosphates, sulfates and silicates, have recently received widespread attention due to their short cutoff edges, stable physicochemical properties and abundant structural types.[7,9,10] A few typical representatives are $NaNH_4PO_3F{\cdot}H_2O$,[26] $(NH_4)_2PO_3F$,[27] $CsSiP_2O_7F$,[28] $La(NH_4)(SO_4)_2$,[29] and Li_2BaSiO_4,[30] which show excellent NLO performances. For phosphates, the PO_4 group has a strong interaction with the σ bond and shows transmittance in the UV/deep-UV region.[31] However, according to anionic group theory, the small second-order nonlinear magnetic susceptibility and hyperpolarizability of the PO_4 group easily lead to weak SHG response and small birefringence, presenting a significant hurdle to the widespread applications of phosphates. Until now, the most efficient strategy is to introduce cations with d^0, d^{10} or stereochemically active lone pair (SCALP) electrons. Guided by this idea, a batch of NLO phosphates with large SHG and appropriate birefringence have been presented, such as $LiHgPO_4$ (11 × KDP, 0.068@1064 nm),[32] $Rb_3PbBi(P_2O_7)_2$ (2.8 × KDP, 0.031@1064 nm)[33] and $Ba_3(ZnB_5O_{10})PO_4$ (4 × KDP, 0.04@1064 nm).[34] In general, cations with a similar radius or coordination environment are interchangeable in structure, thereby facilitating the synthesis of compounds with identical

[a]*Key Laboratory of Oil & Gas Fine Chemicals, Ministry of Education and Xinjiang Uyghur Autonomous Region, School of Chemical Engineering and Technology, Xinjiang University, Urumqi 830017, China. E-mail: chenzhaohui@xju.edu.cn*
[b]*Xinjiang Key Laboratory of Solid State Physics and Devices, School of Physical Science and Technology, Xinjiang University, Urumqi 830017, China*
[c]*International Iberian Nanotechnology Laboratory (INL), Braga 4715-330, Portugal*

†Electronic supplementary information (ESI) available: CIF, structural refinement and crystal data, bond valence sums, XRD patterns, SHG responses of all Bi-based phosphates, coordination environment of Bi atoms, UV-Vis-NIR diffuse reflectance spectrum, IR spectrum and TG–DTA curves. CCDC 2219076. For ESI and crystallographic data in CIF or other electronic format see DOI: https://doi.org/10.1039/d3qi00828b

chemical formulae and sustaining similar structural backbone. Our group has recently prepared a series of excellent UV materials $A_3BBi(P_2O_7)_2$ (A = Rb, Cs; B = Pb, Ba) by using an isovalent cation substitution technique.[35]

In this work, we have successfully synthesized β-$Li_2RbBi(PO_4)_2$ within the $Li_2ABi(PO_4)_2$ (A = alkali metal) series, and demonstrated that the well-ordered $^1[Bi_4(PO_4)_8]_\infty$ anionic framework gives rise to a large SHG effect (exptl. 5.2 × KDP). The birefringence of the compound is found to be 0.0348@1064 nm. We also investigated the synthesis, crystal growth, and NLO properties of β-$Li_2RbBi(PO_4)_2$ and discussed its structure–property relationship.

Experiments

Reagents

Rb_2CO_3, Li_2CO_3, LiF, Bi_2O_3, and $NH_4H_2PO_4$ were all purchased from Aladdin Chemistry Co., Ltd and used as received. The purity of all the reagents is 99.9%.

Synthesis

The β-$Li_2RbBi(PO_4)_2$ crystals were grown by the traditional high temperature melt method. The raw reagents, Rb_2CO_3, LiF, Bi_2O_3, and $NH_4H_2PO_4$, were mixed at a molar ratio of 3 : 4 : 3 : 12 and ground homogeneously. The mixture was then placed in a platinum crucible and transferred to a self-assembly furnace. The mixture was heated to 850 °C and maintained for 24 h, followed by slowly cooling down to 500 °C at a rate of 1 °C h^{-1} and further to room temperature at a rate of 20 °C h^{-1}. Finally, the transparent crystals were obtained.

The polycrystalline sample of β-$Li_2RbBi(PO_4)_2$ was prepared *via* a solid-state reaction. A_2CO_3 (A = Li, Rb), Bi_2O_3, and $NH_4H_2PO_4$ were thoroughly mixed in a stoichiometric ratio and then transferred to a corundum crucible. The mixture was heated to 680 °C and maintained for 96 h. The polycrystalline powder of β-$Li_2RbBi(PO_4)_2$ was obtained.

Powder and single-crystal X-ray diffraction

The sample purity of β-$Li_2RbBi(PO_4)_2$ was examined by powder X-ray diffraction (PXRD) using a Bruker D2 PHASER X-ray diffractometer equipped with Cu Kα radiation (λ = 1.5418 Å) at room temperature. The diffraction data were recorded in the 2θ range from 10° to 70°. As shown in Fig. S1a,† the XRD patterns of β-$Li_2RbBi(PO_4)_2$ are in good agreement with the calculated ones derived from the single crystal data.

A single crystal of β-$Li_2RbBi(PO_4)_2$ with dimensions 0.170 × 0.058 × 0.025 mm^3 was selected for structural determination. The diffraction data were collected on a Bruker SMART APEX II charge-coupled device (CCD) diffractometer equipped with graphite-monochromatic Mo-Kα radiation at 273 K, and the integration was carried out using the SAINT program.[36] The numerical absorption was performed using the SADABS program. The positions of the rubidium and bismuth atoms were determined by direct methods using SHELXS-97, and the remaining atoms were located by the full-matrix least-squares technique with anisotropic displacement parameters using the SHELXL-97 program.[37] The lack of symmetry elements of the structure was tested using the PLATON program, and no higher symmetry was found. Further details of structural refinement, atom coordination, equivalent isotropic displacement parameters, bond lengths, bond angles, and anisotropic displacement parameters are listed in Tables S1–S4.†

Thermal behavior analysis

The thermal performance of β-$Li_2RbBi(PO_4)_2$ was determined using a HITACHI STA7300 TG–DTA analyzer instrument under an argon atmosphere from 30 to 1000 °C.

Spectroscopy analysis

The UV-Vis-NIR diffuse reflectance spectrum for β-$Li_2RbBi(PO_4)_2$ was recorded using a Shimadzu SolidSpec-3700DUV spectrophotometer at room temperature. The diffuse reflectance data were converted to absorbance data according to the Kubelka–Munk equation.

The infrared (IR) spectrum was recorded using a Shimadzu IR Affinity-1 Fourier transform infrared spectrometer with wavenumbers ranging from 400 to 4000 cm^{-1} at room temperature.

SHG measurements

The SHG response of the β-$Li_2RbBi(PO_4)_2$ polycrystalline powder was measured with a Q-switched Nd:YAG laser under 1064 nm using the Kurtz–Perry technology.[38] In order to study the phase matching, the polycrystalline sample was ground and sieved into the following particle size ranges: 25–45, 45–62, 62–75, 75–109, 109–150, and 150–212 μm. The same particle sizes of the KH_2PO_4 (KDP) sample were used as benchmarks.

Details of calculation

To shed light on the relationship between the electronic structure and macroscopic optical properties of β-$Li_2RbBi(PO_4)_2$, the CASTEP calculation software package based on density functional theory (DFT) was used, and the plane wave pseudopotential method was used to calculate the electronic structure and the related optical properties of the single crystal.[39] The calculations were performed using the Perdew–Burke–Ernzerhof (PBE) functional based on the generalized gradient approximation (GGA) and norm-conserving pseudopotentials (NCP).[40–43] The valence electrons were set as Li $1s^2 2s^1$, Rb $4s^2 4p^6 5s^1$, Bi $6s^2 6p^3$, P $3s^2 3p^3$, and O $2s^2 2p^4$. The plane-wave cut-off was set at 830 eV, and the numerical integration of the Brillouin zone was performed using 3 × 5 × 1 Monkhorst–Pack *k*-point sampling. The structure of β-$Li_2RbBi(PO_4)_2$ was optimized with the convergence criteria of the total energy, maximum ionic force, maximum ionic displacement, and maximum stress being 5 × 10^{-6} eV per atom, 1 × 10^{-2} eV $Å^{-1}$, 5 × 10^{-4} Å, and 2 × 10^{-2} GPa, respectively. The refractive indices and birefringence were further calculated using the OptaDOS code.[44,45] The NLO coefficients were calculated using the "sum over states" (SOS) expressions.[46,47] The SHG-weighted densities

were obtained to assess the influence of different groups on the nonlinearity of the title compound.

Results and discussion

Crystal structure

β-$Li_2RbBi(PO_4)_2$ crystallizes in the non-centrosymmetric (NCS) monoclinic space group $P2_1$ (no. 4). There is another phase of $Li_2RbBi(PO_4)_2$ reported by Wen *et al.*,[48] which we named α-$Li_2RbBi(PO_4)_2$ here to discriminate the two types of compounds. Its asymmetric units contain four Li, two Rb, two Bi, four P, and sixteen O atoms. It is noteworthy that β-$Li_2RbBi(PO_4)_2$ has oxygen atoms in disordered positions and each O(15) and O(16) atomic position is divided into two parts, O(15A)–O(15B) and O(16A)–O(16B). There are four crystallographically independent P atoms, which are bound to four O atoms to form the $[PO_4]^{3-}$ tetrahedron with the P–O bonds in the range from 1.475(16) to 1.76(2) Å. The Bi atoms are coordinated with five or seven oxygen atoms to build $Bi(1)O_5$ and $Bi(2)O_7$ polyhedra, which are further interconnected to form a 1D $^1[Bi_2O_{11}]_\infty$ chain with the Bi–O distance between 2.153(6) and 2.734(9) Å (Fig. 1a). Specifically, three adjacent PO_4 tetrahedra connect to one $Bi(1)O_5$ polyhedron *via* a corner-sharing connection mode, and another $P(3)O_4$ tetrahedron connects to one $Bi(2)O_7$ polyhedron by edge-sharing, yielding 1D $^1[Bi_4(PO_4)_8]_\infty$ chains along the *b* direction (Fig. 1b and S2†). Li atoms also have two coordination modes: the $Li(1–3)O_4$ tetrahedron, which is interconnected by corner-sharing to form the $^1[Li_3O_{10}]_\infty$ chain, and the $Li(4)O_5$ polyhedron, which is interconnected by corner-sharing O(16B) to form the $^1[Li_2O_9]_\infty$ chain with the Li–O distance between 1.855(15) and 2.65(3) Å (Fig. 1c). The 1D $^1[Bi_4(PO_4)_8]_\infty$ chains are further interconnected with two types of Li–O chains to form a 3D framework with Rb atoms filling in the gaps to balance the charge (Fig. 1d). The calculated bond valence states of Li, Rb, Bi, P, and O atoms are 1.14–1.13, 1.19–1.26, 2.56–2.73, 4.76–4.99, and 1.8–2.15, respectively, in agreement with the corresponding expected oxidation states of +1, +1, +3, +5, and −2 (Tables S3 and S5†).

Notably, α-$Li_2RbBi(PO_4)_2$ crystallizes in the *C*2 space group, while β-$Li_2RbBi(PO_4)_2$ crystallizes in the $P2_1$ space group. They have similar Bi–P–O chain configurations. Structurally, β-$Li_2RbBi(PO_4)_2$ differs from α-$Li_2RbBi(PO_4)_2$ in the following aspects: (1) the width of the $^1[Bi_3P_6O_{30}]_\infty$ chain in α-$Li_2RbBi(PO_4)_2$ is 15.243 Å, which is composed of isolated $[Bi_3O_{16}]$ clusters and $[PO_4]$ groups, while that of the $^1[Bi_4(PO_4)_8]_\infty$ chain in β-$Li_2RbBi(PO_4)_2$ is 19.654 Å, which is composed of more compactly stacked $^1[Bi_2O_{11}]_\infty$ chains and $[PO_4]$ groups (Fig. 1e and f). (2) The PO_4 groups in α-$Li_2RbBi(PO_4)_2$ and β-$Li_2RbBi(PO_4)_2$ are both highly ordered, but the angle between the terminal PO_4 polyhedra of $^1[Bi_4(PO_4)_8]_\infty$ along the *b*-axis in β-$Li_2RbBi(PO_4)_2$ is 101.4°, while the angle of $^1[Bi_3P_6O_{30}]_\infty$ in α-$Li_2RbBi(PO_4)_2$ is 104.68°. (3) The PO_4 groups of Bi–P–O chains in β-$Li_2RbBi(PO_4)_2$ are more closely aligned in parallel along the *b*-axis and such microscopic stacking of PO_4 in β-$Li_2RbBi(PO_4)_2$ may be more favorable for inducing a strong SHG effect. In contrast, the broadening of the Bi–P–O chains in β-$Li_2RbBi(PO_4)_2$ increases the density of $[PO_4]^{3-}$ units, thereby making the average number of connected PO_4 tetrahedra per Bi–O polyhedron increase from three to four. In addition, the PO_4 groups are arranged in a more ordered manner in β-$Li_2RbBi(PO_4)_2$ than α-$Li_2RbBi(PO_4)_2$, which is favorable for improving the second-order nonlinear magnetization and hyperpolarization.

Spectroscopy analysis

The infrared spectrum of β-$Li_2RbBi(PO_4)_2$ is shown in Fig. S3a.† The wide absorption bands at 1195–1028 cm^{-1} rep-

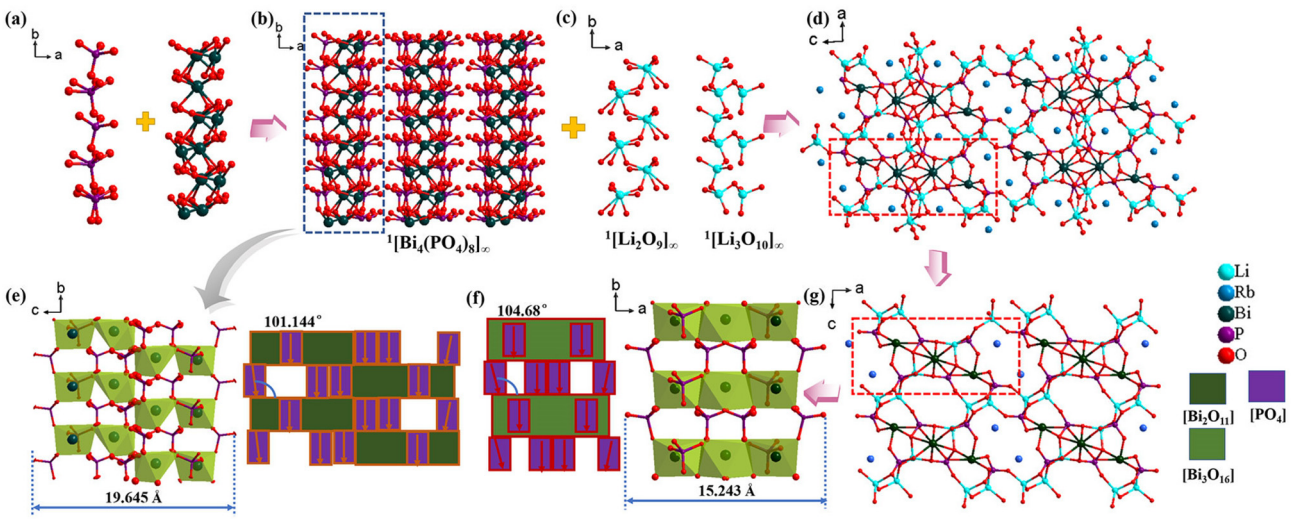

Fig. 1 (a) Optimally aligned arrangement of $[PO_4]$ and $^1[Bi_2O_{11}]_\infty$ units in β-$Li_2RbBi(PO_4)_2$. (b) 1D infinite $^1[Bi_4(PO_4)_8]_\infty$ chain. (c) 1D infinite $^1[Li_2O_9]_\infty$ and $^1[Li_3O_{10}]_\infty$ chains. (d) Crystal structure of β-$Li_2RbBi(PO_4)_2$. (e and f) Chain width and modular description of the 1D infinite $^1[Bi_4(PO_4)_8]_\infty$ chain in β-$Li_2RbBi(PO_4)_2$ (e) and the 1D infinite $^1[Bi_3(PO_4)_6]_\infty$ chain in α-$Li_2RbBi(PO_4)_2$ (f). (g) Crystal structure of α-$Li_2RbBi(PO_4)_2$.

resent the P–O stretching vibrations. The peaks at 579, 510, and 460 cm^{-1} are attributed to the basic frequency of the PO_4 group.[48] The UV-Vis-NIR diffuse reflectance spectrum is shown in Fig. S3b.† The UV cutoff edge of β-$Li_2RbBi(PO_4)_2$ is about 276 nm, indicating that β-$Li_2RbBi(PO_4)_2$ is an UV optical crystal.

Thermal behavior and phase transition analysis

Analysis of the thermogravimetric (TG) curve of β-$Li_2RbBi(PO_4)_2$ shows that it has no significant weight loss from 30 to 1000 °C (Fig. S4†), indicating its good thermal stability. Further differential thermal analysis (DTA) reveals a sharp endothermic peak at 729 °C during the heating process and an obvious exothermic peak at 739 °C during the cooling process. The XRD patterns are inconsistent for β-$Li_2RbBi(PO_4)_2$ before and after melting (Fig. S1b†), implying that the compound is incongruent and the appropriate flux is needed in crystal growth.

To probe the phase transition and melting point of the compound, we have synthesized the pure phases of α-$Li_2RbBi(PO_4)_2$ and β-$Li_2RbBi(PO_4)_2$ by the high-temperature solid-state method. We conducted the XRD phase analysis on sintered samples at different centigrade temperatures (Fig. S1c†), and found that the sample at 650 °C is the α-$Li_2RbBi(PO_4)_2$ phase while the sample at 680 °C corresponds to β-$Li_2RbBi(PO_4)_2$, indicating that β-$Li_2RbBi(PO_4)_2$ is a high-temperature phase and α-$Li_2RbBi(PO_4)_2$ is a low-temperature phase. When the temperature continues to rise to 690 °C, the sample is melted, implying that the sharp exothermic peak at around 729 °C on the heating curve is attributed to the melting point and the endothermic peak at 739 °C could be the overlap of the phase transition peak and melting peak due to the slight temperature difference between the two peaks. We also investigated the XRD pattern of the melted phase and found that the residues are mainly $Rb_4P_2O_7$, Li_3PO_4, BiP_5O_{14}, and Bi_2O_3.

SHG properties

Since β-$Li_2RbBi(PO_4)_2$ crystallizes in the polar space group $P2_1$, we performed SHG measurements, and found that β-$Li_2RbBi(PO_4)_2$ has the largest SHG effect in Bi-based phosphates, about 5.2 × KDP, and can achieve type-I phase matching (Fig. 2a–c and Table S6†). Notably, all the phosphates in the

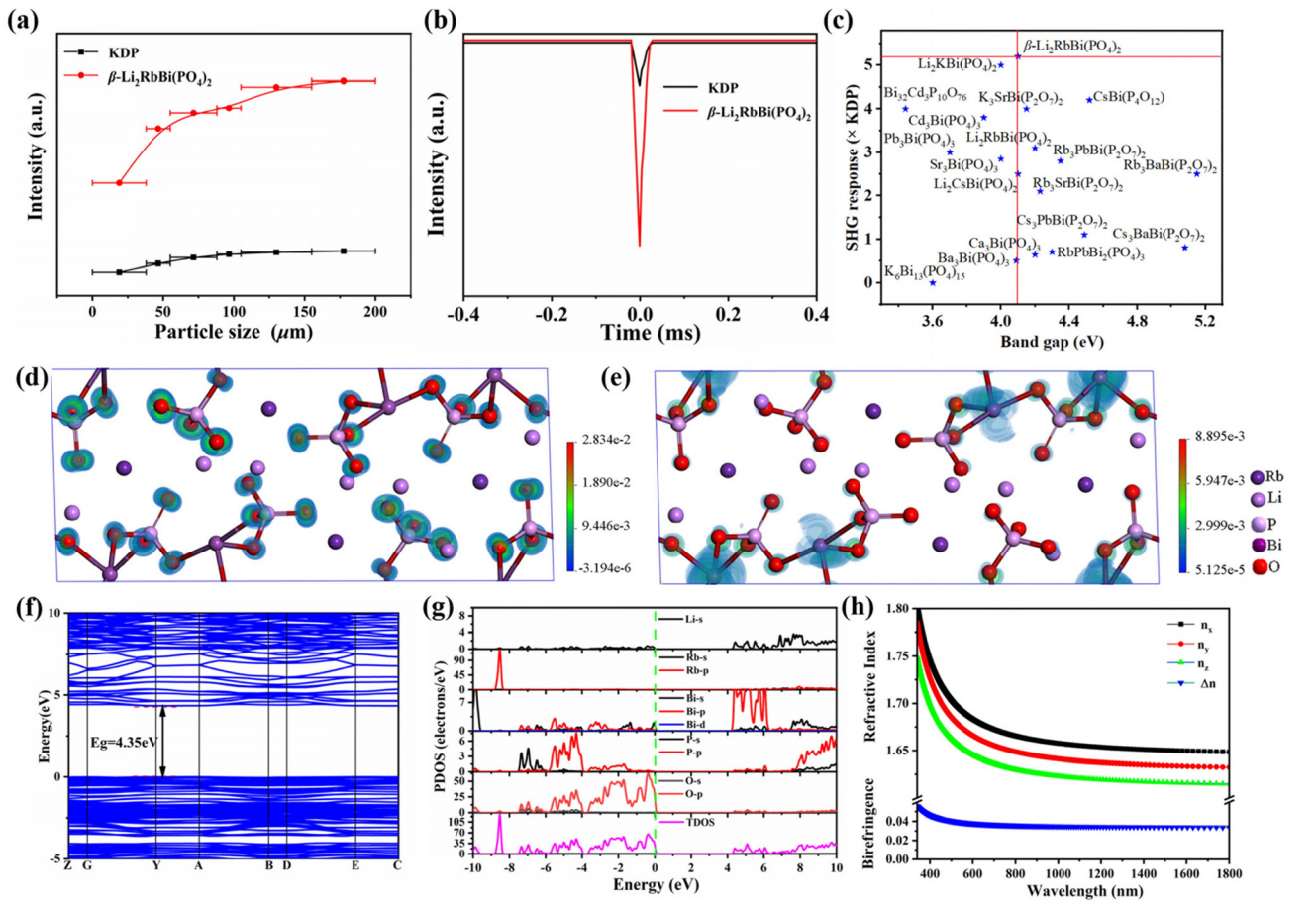

Fig. 2 (a) Phase-matching curves of β-$Li_2RbBi(PO_4)_2$. (b) SHG intensity of β-$Li_2RbBi(PO_4)_2$ and KDP. (c) SHG response of all Bi-based phosphates. (d and e) Veocc (d) and veunocc (e) states of the largest SHG tensor d_{22}. (f) Electronic structure of β-$Li_2RbBi(PO_4)_2$. (g) Density of states (DOS) and projected DOS (PDOS) plots. (h) Refractive indices and birefringence.

$Li_2ABi(PO_4)_2$ (A = K, Rb, and Cs) series exhibit a highly ordered 1D infinite Bi–P–O chain, which helps to enhance the SHG effect. Importantly, the anion basic building block for the compounds in the $P2_1$ space group (such as β-$Li_2RbBi(PO_4)_2$ and $Li_2KBi(PO_4)_2$) evolves from the $^1[Bi_3P_6O_{30}]_\infty$ to $^1[Bi_4(PO_4)_8]_\infty$ chain, and a more parallel arrangement of the PO_4 groups can be noticed when changing from the $C2$ to $P2_1$ space group, thereby contributing to the improvement of the SHG effect.

To gain insight into the effectiveness of the SHG efficiency for β-$Li_2RbBi(PO_4)_2$, we calculated its SHG tensor d_{ij} coefficients. The crystal belongs to the point group 2, and has four independent nonzero SHG coefficients: d_{16} = 1.583 pm V^{-1}, d_{14} = 0.155 pm V^{-1}, d_{22} = −2.536 pm V^{-1}, and d_{23} = 1.104 pm V^{-1}. According to the d_{ij} coefficients of the obtained SHG tensors, the effective SHG (d_{eff}) for β-$Li_2RbBi(PO_4)_2$ is calculated to be 1.45 pm V^{-1} (about 4.41 × KDP), which is comparable to the experimental value (5.2 × KDP). To further quantify the SHG contribution from different building units, we carried out calculations by the real-space atom-cutting technique.[46] Four parts contribute mainly to the d_{eff} of β-$Li_2RbBi(PO_4)_2$: 0.74 pm V^{-1} from P–O, 1.22 pm V^{-1} from Bi–O, 0.370 pm V^{-1} from Li–O, and 0.1 pm V^{-1} from Rb–O groups. Consequently, the distorted BiO_n and PO_4 polyhedra contribute dominantly to the SHG response (Table 1). To better understand the enhanced SHG response of β-$Li_2RbBi(PO_4)_2$, we employed the SHG-density technique to investigate the SHG states in real atomic space (Fig. 2d and e).[49] In the dominant virtual electron process, the main contribution to the largest tensor d_{22} originates from the O 2p orbitals for the occupied states, while it originates from the 6p orbital of SCALP-active Bi^{3+} for the unoccupied states. We also observed that the SHG source of β-$Li_2RbBi(PO_4)_2$ is mainly surrounding the oxygen atoms bridged by P and Bi atoms, which further confirms the synergistic effect of P–O and Bi–O groups in enhancing the total SHG.

Electronic structure and optical properties

To clarify the microscopic mechanism, we carried out first-principles calculations, and found that β-$Li_2RbBi(PO_4)_2$ is a direct transition semiconductor with a band gap of 4.35 eV (Fig. 2f). Fig. 2g shows the total and projected density of states (TDOS/PDOS), where the valence band maximum (VBM) is mainly composed of O 2p and P 3p states and the conduction band minimum (CBM) mainly stems from O 2p, Li 2s, and Bi 6p states. Since β-$Li_2RbBi(PO_4)_2$ crystallizes in a monoclinic crystal system, it has three unequal refractive indices, *e.g.*, n_x, n_y, and n_z. The calculated refractive index curve is $n_x - n_y > n_y - n_z$ in the wavelength range of 300–1800 nm, making it a positive biaxial crystal (Fig. 2h). The birefringence is calculated to be 0.0348@1064 nm, which satisfies the phase matching for β-$Li_2RbBi(PO_4)_2$.

Table 1 The SHG response from various ionic groups obtained by the real-space atom-cutting method for β-$Li_2RbBi(PO_4)_2$

SHG tensors (pm V^{-1})	Origin	Li–O	P–O	Bi–O	Rb–O
d_{16}	1.583	0.122	1.006	1.362	0.494
d_{14}	0.155	0.015	0.350	−0.125	−0.453
d_{22}	−2.535	−1.602	−1.924	−2.201	1.136
d_{23}	1.104	0.571	0.467	0.503	−0.939
d_{eff}	1.450	0.370	0.740	1.220	0.100

Conclusions

We have designed and synthesized a new UV NLO material, β-$Li_2RbBi(PO_4)_2$, and demonstrated that it exhibits the strongest SHG response of 5.2 × KDP among all the Bi-based phosphates. β-$Li_2RbBi(PO_4)_2$ is found to show much improved second-order nonlinear magnetization and hyperpolarization in comparison with α-$Li_2RbBi(PO_4)_2$, which is ascribed to the broadened parallel $^1[Bi_4(PO_4)_8]_\infty$ chains and the more parallel alignment of the PO_4 groups. Further theoretical calculations reveal a synergistic effect of the BiO_n and PO_4 groups in enhancing the SHG effect and birefringence for β-$Li_2RbBi(PO_4)_2$. These findings shall open up an effective avenue in exploring new NLO materials for further enhancing optical performances when needed by manipulating the space group and phase transitional passageway.

Conflicts of interest

There are no conflicts to declare.

Acknowledgements

This work was supported by the National Natural Science Foundation of China (51962033), the Tianshan Talent Project of Xinjiang Uygur Autonomous Region of China (2022TSYCJU0004), and the Xinjiang Major Science and Technology Project (2021A01001-3).

Notes and references

1 P. Becker, Borate Materials in Nonlinear Optics, *Adv. Mater.*, 1998, **10**, 979–992.
2 C. Chen, Y. Wang, B. Wu, K. Wu, W. Zeng and L. Yu, Design and Synthesis of an Ultraviolet-transparent Nonlinear Optical Crystal $Sr_2Be_2B_2O_7$, *Nature*, 1995, **373**, 322–324.
3 B. Wu, D. Tang, N. Ye and C. Chen, Linear and Nonlinear Optical Properties of the $KBe_2BO_3F_2$ (KBBF) Crystal, *Opt. Mater.*, 1996, **5**, 105–109.
4 T. T. Tran, H. Yu, J. M. Rondinelli, K. R. Poeppelmeier and P. S. Halasyamani, Deep Ultraviolet Nonlinear Optical Materials, *Chem. Mater.*, 2016, **28**, 5238–5258.
5 K. M. Ok, Toward the Rational Design of Novel Noncentrosymmetric Materials: Factors Influencing the

Framework Structures, *Acc. Chem. Res.*, 2016, **49**, 2774–2785.
6 M. Mutailipu, K. R. Poeppelmeier and S. Pan, Borates: A Rich Source for Optical Materials, *Chem. Rev.*, 2021, **121**, 1130–1202.
7 S. Bai, D. Wang, H. Liu and Y. Wang, Recent Advances of Oxyfluorides for Nonlinear Optical Applications, *Inorg. Chem. Front.*, 2021, **8**, 1637–1654.
8 J. Chen, C. Hu, F. Kong and J. Mao, High-Performance Second-Harmonic-Generation (SHG) Materials: New Developments and New Strategies, *Acc. Chem. Res.*, 2021, **54**, 2775–2783.
9 W. Huang, S. Zhao and J. Luo, Recent Development of Non-π-Conjugated Deep Ultraviolet Nonlinear Optical Materials, *Chem. Mater.*, 2022, **34**, 5–28.
10 J. Huang, S. Shu and G. Cai, Review of Heteroleptic Tetrahedra as Birefringent or Nonlinear Optical Motifs, *Cryst. Growth Des.*, 2022, **22**, 1500–1514.
11 M. Mutailipu, F. Li, C. Jin, Z. Yang, K. R. Poeppelmeier and S. Pan, Strong Nonlinearity Induced by Coaxial Alignment of Polar Chain and Dense $[BO_3]$ Units in $CaZn_2(BO_3)_2$, *Angew. Chem., Int. Ed.*, 2022, **61**, e202202096.
12 Y. Liu, X. Liu, S. Liu, Q. Ding, Y. Li, L. Li, S. Zhao, Z. Lin, J. Luo and M. Hong, An Unprecedented Antimony(III) Borate with Strong Linear and Nonlinear Optical Responses, *Angew. Chem., Int. Ed.*, 2020, **59**, 7793–7796.
13 J. Song, C. Hu, X. Xu, F. Kong and J. Mao, A Facile Synthetic Route to a New SHG Material with Two Types of Parallel π-Conjugated Planar Triangular Units, *Angew. Chem., Int. Ed.*, 2015, **54**, 3679–3682.
14 G. Zou, C. Lin, H. G. Kim, H. Jo and K. M. Ok, $Rb_2Na(NO_3)_3$: A Congruently Melting UV-NLO Crystal with a Very Strong Second-Harmonic Generation Response, *Crystals*, 2016, **6**, 42.
15 J. Wang, Y. Cheng, H. Wu, Z. Hu, J. Wang, Y. Wu and H. Yu, $Sr_3[SnOSe_3][CO_3]$: A Heteroanionic Nonlinear Optical Material Containing Planar π-conjugated $[CO_3]$ and Heteroleptic $[SnOSe_3]$ Anionic Groups, *Angew. Chem., Int. Ed.*, 2022, **61**, e202201616.
16 M. Luo, G. Wang, C. Lin, N. Ye, Y. Zhou and W. Cheng, $Na_4La_2(CO_3)_5$ and $CsNa_5Ca_5(CO_3)_8$: Two New Carbonates as UV Nonlinear Optical Materials, *Inorg. Chem.*, 2014, **53**, 8098–8104.
17 C. Chen, Y. Wu, A. Jiang, B. Wu, G. You, R. Li and S. Lin, New Nonlinear-optical crystal: LiB_3O_5, *J. Opt. Soc. Am. B*, 1989, **6**, 616–621.
18 C. Chen, B. Wu, A. Jiang and G. You, A New-type Ultraviolet SHG Crystal—β-BaB_2O_4, *Sci. Sin., Ser. B*, 1985, **28**, 235–243.
19 Y. Wang, B. Zhang, Z. Yang and S. Pan, Cation-Tuned Synthesis of Fluorooxoborates: Towards Optimal Deep-Ultraviolet Nonlinear Optical Materials, *Angew. Chem., Int. Ed.*, 2018, **57**, 2150–2154.
20 Z. Zhang, Y. Wang, B. Zhang, Z. Yang and S. Pan, Polar Fluorooxoborate, NaB_4O_6F: A Promising Material for Ionic Conduction and Nonlinear Optics, *Angew. Chem., Int. Ed.*, 2018, **57**, 6577–6581.
21 F. Liang, L. Kang, P. Gong, Z. Lin and Y. Wu, Rational Design of Deep-Ultraviolet Nonlinear Optical Materials in Fluorooxoborates: Toward Optimal Planar Configuration, *Chem. Mater.*, 2017, **29**, 7098–7102.
22 M. Mutailipu, M. Zhang, B. Zhang, L. Wang, Z. Yang, X. Zhou and S. Pan, $SrB_5O_7F_3$ Functionalized with $[B_5O_9F_3]_6$ Chromophores: Accelerating the Rational Design of Deep-Ultraviolet Nonlinear Optical Materials, *Angew. Chem., Int. Ed.*, 2018, **57**, 6095–6099.
23 M. Xia, F. Li, M. Mutailipu, S. Han, Z. Yang and S. Pan, Discovery of First Magnesium Fluorooxoborate with Stable Fluorine Terminated Framework for Deep-UV Nonlinear Optical Application, *Angew. Chem., Int. Ed.*, 2021, **60**, 14650–14656.
24 G. Zou, N. Ye, L. Huang and X. Lin, Alkaline-Alkaline Earth Fluoride Carbonate Crystals $ABCO_3F$ (A = K, Rb, Cs; B = Ca, Sr, Ba) as Nonlinear Optical Materials, *J. Am. Chem. Soc.*, 2011, **133**, 20001–20007.
25 T. T. Tran, J. Young, J. M. Rondinelli and P. S. Halasyamani, Mixed-Metal Carbonate Fluorides as Deep-Ultraviolet Nonlinear Optical Materials, *J. Am. Chem. Soc.*, 2017, **139**, 1285–1295.
26 L. Xiong, J. Chen, J. Lu, C. Pan and L. Wu, Monofluorophosphates: A New Source of Deep-Ultraviolet Nonlinear Optical Materials, *Chem. Mater.*, 2018, **30**, 7823–7830.
27 B. Zhang, G. Han, Y. Wang, X. Chen, Z. Yang and S. Pan, Expanding Frontiers of Ultraviolet Nonlinear Optical Materials with Fluorophosphates, *Chem. Mater.*, 2018, **30**, 5397–5403.
28 Q. Ding, X. Liu, S. Zhao, Y. Wang, Y. Li, L. Li, S. Liu, Z. Lin, M. Hong and J. Luo, Designing a Deep-UV Nonlinear Optical Fluorooxosilicophosphate, *J. Am. Chem. Soc.*, 2020, **142**, 6472–6476.
29 C. Wu, X. Jiang, Y. Hu, C. Jiang, T. Wu, Z. Lin, Z. Huang, M. G. Humphrey and C. Zhang, A Lanthanum Ammonium Sulfate Double Salt with a Strong SHG Response and Wide Deep-UV Transparency, *Angew. Chem., Int. Ed.*, 2022, **61**, e202115855.
30 H. Wu, B. Zhang, H. Yu, Z. Hu, J. Wang, Y. Wu and P. S. Halasyamani, Designing Silicates as Deep-UV Nonlinear Optical (NLO) Materials using Edge-Sharing Tetrahedra, *Angew. Chem., Int. Ed.*, 2020, **59**, 8922–8926.
31 L. Li, Y. Wang, B. Lei, S. Han, Z. Yang, K. R. Poeppelmeier and S. Pan, A New Deep-Ultraviolet Transparent Orthophosphate $LiCs_2PO_4$ with Large Second Harmonic Generation Response, *J. Am. Chem. Soc.*, 2016, **138**, 9101–9104.
32 B. Wu, C. Hu, F. Mao, R. Tang and J. Mao, Highly Polarizable Hg^{2+} Induced a Strong Second Harmonic Generation Signal and Large Birefringence in $LiHgPO_4$, *J. Am. Chem. Soc.*, 2019, **141**, 10188–10192.
33 X. Lu, Z. Chen, X. Shi, Q. Jing and M. Lee, Two Pyrophosphates with Large Birefringences and Second-Harmonic Responses as Ultraviolet Nonlinear Optical Materials, *Angew. Chem., Int. Ed.*, 2020, **59**, 17648–17656.

34 H. Yu, J. Cantwell, H. Wu, W. Zhang, K. R. Poeppelmeier and P. S. Halasyamani, Top-Seeded Solution Crystal Growth, Morphology, Optical and Thermal Properties of $Ba_3(ZnB_5O_{10})PO_4$, *Cryst. Growth Des.*, 2016, **16**, 3976–3982.

35 L. Qi, Z. Chen, X. Shi, X. Zhang, Q. Jing, N. Li, Z. Jiang, B. Zhang and M. Lee, $A_3BBi(P_2O_7)_2$ (A = Rb, Cs; B = Pb, Ba): Isovalent Cation Substitution to Sustain Large Second-Harmonic Generation Responses, *Chem. Mater.*, 2020, **32**, 8713–8723.

36 *SAINT, version 7.60A*, Bruker Analytical X-ray Instruments, Inc., Madison, WI, 2008.

37 G. M. Sheldrick, Crystal structure refinement with SHELXL, *Acta Crystallogr., Sect. C: Struct. Chem.*, 2015, **71**, 3–8.

38 S. Kurtz and T. Perry, A Powder Technique for the Evaluation of Nonlinear Optical Materials, *J. Appl. Phys.*, 1968, **39**, 3798–3813.

39 S. J. Clark, M. D. Segall, C. J. Pickard, P. J. Hasnip, M. I. J. Probert, K. Refson and M. C. Payne, First Principles Methods Using CASTEP, *Zeitschrift für Kristallographie - Crystalline Materials*, 2005, **220**, 567–570.

40 M. Ernzerhof and G. E. Scuseria, Assessment of the Perdew–Burke–Ernzerhof Exchange-Correlation Functional, *J. Chem. Phys.*, 1999, **110**, 5029–5036.

41 J. P. Perdew, K. Burke and M. Ernzerhof, Generalized Gradient Approximation Made Simple, *Phys. Rev. Lett.*, 1996, **77**, 3865–3868.

42 A. M. Rappe, K. M. Rabe, E. Kaxiras and J. D. Joannopoulos, Optimized Pseudopotentials, *Phys. Rev. B: Condens. Matter Mater. Phys.*, 1990, **41**, 1227–1230.

43 D. R. Hamann, M. Schlüter and C. Chiang, Norm-Conserving Pseudopotentials, *Phys. Rev. Lett.*, 1979, **43**, 1494–1497.

44 A. J. Morris, R. J. Nicholls, C. J. Pickard and J. R. Yates, OptaDOS: A Tool for Obtaining Density of States, Core-level and Optical Spectra from Electronic Structure Codes, *Comput. Phys. Commun.*, 2014, **185**, 1477–1485.

45 R. J. Nicholls, A. J. Morris, C. J. Pickard and J. R. Yates, OptaDOS: a new tool for EELS calculations, *J. Phys.: Conf. Ser.*, 2012, **371**, 012062.

46 J. Lin, M. Lee, Z. Liu, C. Chen and C. J. Pickard, Mechanism for Linear and Nonlinear Optical Effects in β-BaB_2O_4 Crystals, *Phys. Rev. B: Condens. Matter Mater. Phys.*, 1999, **60**, 13380–13389.

47 B. Zhang, M. Lee, Z. Yang, Q. Jing, S. Pan, M. Zhang, H. Wu, X. Su and C. Li, Simulated Pressure-induced Blue-shift of Phase-matching Region and Nonlinear Optical Mechanism for $K_3B_6O_{10}X$ (X = Cl, Br), *Appl. Phys. Lett.*, 2015, **106**, 031906.

48 M. Wen, C. Hu, H. Wu, Z. Yang, H. H. Yu and S. Pan, Three non-centrosymmetric bismuth phosphates, $Li_2ABi(PO_4)_2$ (A = K, Rb, and Cs): Effects of Cations on the Crystal Structure and SHG Response, *Inorg. Chem. Front.*, 2020, **7**, 3364–3370.

49 M. Lee, C. Yang and J. Jan, Band-resolved Analysis of Nonlinear Optical Properties of Crystalline and Molecular Materials, *Phys. Rev. B: Condens. Matter Mater. Phys.*, 2004, **70**, 235110.

